

Sixty years of radiocarbon dioxide measurements at Wellington, New Zealand 1954 – 2014

Jocelyn C. Turnbull^{1,2,*}, Sara E. Mikaloff Fletcher³, India Ansell¹, Gordon Brailsford³, Rowena Moss³, Margaret Norris¹, Kay Steinkamp³

¹GNS Science, Rafter Radiocarbon Laboratory, Lower Hutt, New Zealand

²CIRES, University of Colorado at Boulder, Boulder, Colorado, USA

³NIWA, Wellington, New Zealand

* contact author: j.turnbull@gns.cri.nz

1. Abstract

We present 60 years of $\Delta^{14}\text{CO}_2$ measurements from Wellington, New Zealand (41°S, 175°E). The record has been extended and fully revised. New measurements have been used to evaluate the existing record and to replace original measurements where warranted. This is the earliest direct atmospheric $\Delta^{14}\text{CO}_2$ record and records the rise of the ^{14}C “bomb spike”, the subsequent decline in $\Delta^{14}\text{CO}_2$ as bomb ^{14}C moved throughout the carbon cycle and increasing fossil fuel CO_2 emissions further decreased atmospheric $\Delta^{14}\text{CO}_2$. The initially large seasonal cycle in the 1960s reduces in amplitude and eventually reverses in phase, resulting in a small seasonal cycle of about 2 ‰ in the 2000s. The seasonal cycle at Wellington is dominated by the seasonality of cross-tropopause transport, and differs slightly from that at Cape Grim, Australia, which is influenced by anthropogenic sources in winter. $\Delta^{14}\text{CO}_2$ at Cape Grim and Wellington show very similar trends, with significant differences only during periods of known measurement uncertainty. In contrast, similar clean air sites in Northern Hemisphere show a higher and earlier bomb ^{14}C peak, consistent with a 1.4-year interhemispheric exchange time. From the 1970s until the early 2000s, the Northern and Southern Hemisphere $\Delta^{14}\text{CO}_2$ were quite similar, apparently due to the balance of ^{14}C -free fossil fuel CO_2 emissions in the north and ^{14}C -depleted ocean upwelling in the south. The Southern Hemisphere sites show a consistent and marked elevation above the Northern Hemisphere sites since the early 2000s, which is most likely due to reduced upwelling of ^{14}C -depleted and carbon-rich deep waters in the Southern Ocean, although an underestimate of fossil fuel CO_2 emissions or changes in biospheric exchange are also possible explanations. This developing $\Delta^{14}\text{CO}_2$ interhemispheric gradient is consistent with recent studies that indicate a reinvigorated Southern Ocean carbon sink since the mid-2000s, and suggests that upwelling of deep waters plays an important role in this change.

37 2. Introduction

38 Measurements of radiocarbon in atmospheric carbon dioxide ($\Delta^{14}\text{CO}_2$) have long been
39 used as a key to understanding the global carbon cycle. The first atmospheric $\Delta^{14}\text{CO}_2$
40 measurements were begun at Wellington, New Zealand in 1954 (Rafter, 1955; Rafter et
41 al., 1959), aiming to better understand carbon exchange processes (Otago Daily Times,
42 1957). Northern Hemisphere $\Delta^{14}\text{CO}_2$ measurements began a few years later in 1962, in
43 Norway (Nydal and Løvseth, 1983) and 1959 in Austria (Levin et al., 1985).

44
45 ^{14}C is a cosmogenic nuclide produced naturally in the upper atmosphere through neutron
46 spallation, reacts rapidly to form ^{14}CO and then oxidizes to $^{14}\text{CO}_2$ over a period of 1- 2
47 months, after which it moves throughout the global carbon cycle. Natural ^{14}C production
48 is roughly balanced by radioactive decay, which mostly occurs in the carbon-rich and
49 slowly overturning ocean carbon reservoir and to a lesser extent in the faster cycling
50 terrestrial carbon reservoir. The perturbations to $\Delta^{14}\text{CO}_2$ from atmospheric nuclear
51 weapons testing in the mid-20th century and additions of ^{14}C -free CO_2 from fossil fuel
52 burning have both provided tools to investigate CO_2 sources and sinks.

53
54 Penetration of bomb- ^{14}C into the oceans has been used to understand ocean carbon uptake
55 processes (Oeschger et al., 1975; Broecker et al., 1985; Key et al., 2004; Naegler et al.,
56 2006; Sweeney et al., 2007). Terrestrial biosphere carbon residence times and exchange
57 processes have also been widely investigated using bomb- ^{14}C (e.g. Trumbore et al., 2000;
58 Naegler et al., 2009). Stratospheric residence times, cross-tropopause transport and
59 interhemispheric exchange can also be examined with atmospheric $\Delta^{14}\text{CO}_2$ observations
60 (Kjellström et al., 2000; Kanu et al., 2015).

61
62 The Suess Effect, the decrease in atmospheric $\Delta^{14}\text{CO}_2$ due to the addition of ^{14}C -free
63 fossil fuel CO_2 , was first identified in 1955 (Suess, 1955). It has subsequently been
64 refined (Meijer et al., 1996; Levin et al., 2003; Turnbull et al., 2006) and used to
65 investigate fossil fuel CO_2 additions at various scales (e.g. Turnbull et al., 2009a; Djuricin
66 et al., 2010; Miller et al., 2012; Lopez et al., 2013; Turnbull et al., 2015).

67
68 The full atmospheric ^{14}C budget has been investigated using long term $\Delta^{14}\text{CO}_2$ records in
69 conjunction with atmospheric transport models (Caldiera et al., 1998; Randerson et al.,
70 2002; Naegler et al., 2006; Turnbull et al., 2009b; Levin et al., 2010). These have shown
71 changing controls on $\Delta^{14}\text{CO}_2$ through time. Prior to nuclear weapons testing, natural
72 cosmogenic production added ^{14}C in the upper atmosphere, which reacted to CO_2 and
73 moved throughout the atmosphere and the carbon cycle. The short carbon residence time
74 in the biosphere meant that biospheric exchange processes had only a small influence on
75 $\Delta^{14}\text{CO}_2$, whereas the ocean exerted a stronger influence due to radioactive decay during
76 its much longer (and temporally varying) turnover time. The addition of bomb ^{14}C in the
77 1950s and 1960s almost doubled the atmospheric ^{14}C content. This meant that both the
78 ocean and biosphere were very ^{14}C -poor relative to the atmosphere in the two decades
79 following the atmospheric test ban treaty. As the bomb- ^{14}C was distributed throughout
80 the carbon cycle, this impact weakened, and by the 1990s, the additions of fossil fuel CO_2
81 became the largest contributor to the $\Delta^{14}\text{CO}_2$ trend (Randerson et al., 2002; Turnbull et
82 al., 2007; Levin et al., 2010; Graven et al., 2012).

83

84 The long-term $\Delta^{14}\text{CO}_2$ records have been crucial in all of these findings, and the
85 Wellington $\Delta^{14}\text{CO}_2$ record is of special importance, being the oldest direct atmospheric
86 trace gas record, even predating the CO_2 mole fraction record started at Mauna Loa in
87 1958 (Keeling, 1961; Keeling and Whorf, 2005). It is the only Southern Hemisphere
88 record recording the bomb spike. Several short Southern Hemisphere records do exist
89 (Manning et al., 1990; Meijer et al., 2006; Graven et al., 2012b; Hua and Barbetti, 2013),
90 and some longer records began in the 1980s (Levin et al., 2010). Over the more than 60
91 years of measurement, there have necessarily been changes in how the Wellington
92 samples are collected and measured. There are no comparable records during the first 30
93 years of measurement, so that the data quality has not been independently evaluated.
94 Comparison with other records since the mid-1980s has suggested that there may be
95 biases in some parts of the Wellington record (Currie et al., 2011).

96

97 Here we present a revised and extended Wellington atmospheric $^{14}\text{CO}_2$ record, spanning
98 60 years from December 1954 to December 2014. We detail the different sampling,
99 preparation and measurement techniques used through the record, compare with new tree
100 ring measurements, discuss revisions to the previously published data and provide a final
101 dataset with accompanying smooth curve fit.

102

103 In the results and discussion, we revisit the key findings that the Wellington $^{14}\text{CO}_2$ record
104 has provided over the years and expand with new findings based on the most recent part
105 of the record. The most recent publication of this dataset included data to 2005 (Currie et
106 al., 2011) and showed periods of variability and a seasonal cycle at Wellington that differ
107 markedly from the independent Cape Grim, Tasmania $^{14}\text{CO}_2$ record at a similar southern
108 latitude (Levin et al., 2010). Here we add complementary new data to investigate these
109 differences, fill gaps and extend the record to near-present.

110 3. Methods

111 Over 60 years of measurement, a number of different sample collection, preparation,
112 measurement and reporting methods have been used. In this section, we give an
113 overview of the various methods and changes through time, and they are summarized in
114 table 1. Full details of the sampling methods used through time are provided in the
115 supplementary material, compiling methodological information documented in previous
116 reports on the Wellington record (Rafter and Fergusson, 1959; Manning et al., 1990;
117 Currie et al., 2011) along with methods newly applied in this new extension and
118 refinement of the dataset.

119

120 3.1. Sampling sites

121 Samples from 15 December 1954 – 5 June 1987 were collected at Makara (Lowe, 1974),
122 on the south-west coast of the North Island of New Zealand (MAK, 41.25°S, 174.69°E,
123 300 m asl). Samples since 8 July 1988 have been collected at Baring Head (Brailsford et
124 al., 2012) on the South Coast of the lower North Island and 23 km southeast of Makara
125 (BHD, 41.41°S, 174.87°E, 80 m asl) (figure 1). We also discuss tree ring samples
126 collected from Eastbourne, 12 km north of Baring Head on Wellington Harbour.

127

128 3.2. Collection methods

129 3.2.1. NaOH absorption

130 The primary collection method is static absorption of CO₂ into nominally CO₂-free 0.5 or
131 1 M sodium hydroxide (NaOH) solution, which is left exposed to air at the sampling site
132 providing an integrated sample over a period of ~2 weeks (section S3.1; Rafter, 1955).
133 From 1954-1995, ~ 2 L NaOH solution was exposed to air in a large (~450 cm² surface
134 area) Pyrex® tray. Since 1995, wide-mouth high-density polyethylene (HDPE) bottles
135 containing ~200 mL NaOH solution were left open inside a Stevenson meteorological
136 screen; the depth of the solution in the bottles remained the same as that in the previously
137 used trays. No significant difference has been observed between the two methods (Currie
138 et al., 2011). A few early (1954-1970) samples were collected using different vessels, air
139 pumped through the NaOH (vs. passive absorption), or NaOH was replaced with barium
140 hydroxide (Rafter, 1955; Manning et al., 1990). CO₂ is extracted from the NaOH solution
141 by acidification followed by cryogenic distillation (Rafter and Fergusson, 1959; Currie et
142 al., 2011). Static NaOH absorption necessarily fractionates relative to CO₂ in the
143 atmosphere. Typical δ¹³C values are -15 to -25 ‰ for these samples, and this is corrected
144 for in the data analysis.

145

146 3.2.2. Whole air flasks

147 In this study, we use whole air flask samples collected at Baring Head to supplement
148 and/or replace NaOH samples. Flasks of whole air are collected by flushing ambient air
149 through the flask for several minutes then filled to slightly over ambient pressure. Most
150 flasks were collected during southerly, clean air conditions (Stephens et al., 2013). CO₂
151 is extracted cryogenically (Turnbull et al., 2015). For whole air samples collected from
152 1984-1993, the extracted CO₂ was archived until 2012. We evaluated the quality of this
153 archived CO₂ using two methods. Tubes with major leakage were readily detected by air
154 present in the tube and were discarded. δ¹³C from all the remaining samples was in
155 agreement with δ¹³C measured from separate flasks collected at Baring Head and
156 measured for δ¹³C by Scripps Institution of Oceanography at close to the time of
157 collection (<http://scrippsco2.ucsd.edu/data/nzd>). Whole air samples collected since 2013
158 are analyzed for δ¹³C and other trace gases and isotopes at NIWA (Ferretti et al., 2000)
159 and for the ¹⁴CO₂ measurement, CO₂ is extracted from whole air at Rafter Radiocarbon
160 Laboratory (Turnbull et al., 2015).

161

162 3.2.3. Tree rings

163 When trees photosynthesize, they faithfully record the Δ¹⁴C of ambient CO₂ in their
164 cellulose, the structural component of wood. Annual tree rings therefore provide a
165 summertime (approximately September – April in the Southern Hemisphere) daytime
166 average Δ¹⁴CO₂. Photosynthetic uptake varies during the daylight hours depending on
167 factors including growth period, sunlight, and temperature (Bozhinova et al., 2013),
168 resulting in a somewhat different effective sampling pattern than the 1-2 week NaOH
169 solution collections. We show in section 3.5.1. that at the Wellington location this
170 difference is negligible. Note that we assign the mean age of each ring as January 1 of the
171 year in which growth finished (i.e. the mean age of a ring growing from September –
172 April), whereas dendrochronologists assign the “ring year” as the year in which ring
173 growth started (i.e. the previous year).

174
175 We collected cores from three trees close to the Baring Head site. A pine (*Pinus radiata*)
176 located 10 m from the Baring Head sampling station (figure 1) yielded rings back to 1986
177 (Norris, 2015). A longer record was obtained from two New Zealand kauri (*Agathis*
178 *australis*) specimens planted in 1919 and 1920, located 20 m from one another in
179 Eastbourne, 12 km from Baring Head (figure 1). Kauri is a long-lived high-density
180 softwood species that has been widely used in dendrochronology and radiocarbon
181 calibration studies (e.g. Hogg et al., 2013).

182
183 Annual rings were counted from each core. Shifting the Eastbourne record by one year in
184 either direction moves the ^{14}C bomb spike maximum out of phase with the NaOH-based
185 Wellington $\Delta^{14}\text{CO}_2$ record (supplementary figure S1), confirming that the ring counts are
186 correct. For the Baring Head pine, rings go back to only 1986, and we verify them by
187 comparing with the Eastbourne record. They show an insignificant mean difference of -
188 0.4 ± 0.8 ‰ (supplementary figure S1).

189
190 In practice, it is difficult to ensure that one annual ring is sampled without losing any
191 material from that ring, and no wood from surrounding rings is included. To evaluate the
192 potential bias from this source, we measured replicate samples from different cores from
193 the same tree (Baring Head) or two different trees (Eastbourne). For samples collected
194 since 1985, all these replicates are consistent within their assigned uncertainties
195 (supplementary figure S2). However, for three replicates from Eastbourne in 1963, 1965
196 and 1971, we see large differences of 9.2, 44.5 and 4.9 ‰, which we attribute to small
197 differences in sampling of the rings that were magnified by the rapid change in $\Delta^{14}\text{C}$ of
198 up to 200 ‰ yr^{-1} during this period. Thus, the tree ring $\Delta^{14}\text{C}$ values during this period
199 should be treated with caution.

200
201 Cellulose was isolated from whole tree rings by first removing labile organics with
202 solvent washes, then oxidation to isolate the cellulose from other materials (Norris, 2015;
203 Hua et al., 2000). The cellulose was combusted and the CO_2 purified following standard
204 methods in the Rafter Radiocarbon Laboratory (Baisden et al., 2013).

205

206 3.3. ^{14}C measurement

207 Static NaOH samples were measured by conventional decay counting on the CO_2 gas
208 from 1954 – 1995 (Manning et al., 1990; Currie et al., 2011) and these are identified by
209 their unique “NZ” numbers. All measurements made since 1995, including recent
210 measurements of flask samples collected in the 1980s and 1990s, were reduced to
211 graphite, measured by accelerator mass spectrometry (AMS), and are identified by their
212 unique “NZA” numbers. The LG1 graphitization system was used from 1995 to 2011
213 (NZA < 50,000) (Lowe et al., 1987), and replaced with the RG20 graphite system in 2011
214 (NZA > 50,000) (Turnbull et al., 2015). Samples measured by AMS were stored for up
215 to three years between sample collection and extraction/graphitization/measurement.

216

217 For samples collected from 1995 to 2010, an EN Tandem AMS was used for
218 measurement (NZA < 35,000, Zondervan and Sparks, 1996). Until 2005 (NZA < 30,000,
219 including all previously reported Wellington $^{14}\text{CO}_2$ data), only ^{13}C and ^{14}C were

220 measured on the EN Tandem system, so the normalization correction for isotopic
221 fractionation (Stuiver and Polach, 1977) was performed using an offline isotope ratio
222 mass spectrometer $\delta^{13}\text{C}$ value. The data reported from 2005 onwards (NZA > 30,000)
223 show a reduction in scatter reflecting the addition of online ^{12}C measurement in the EN
224 Tandem system in 2005. This allows direct online correction for isotopic fractionation
225 that may occur during sample preparation and in the AMS system (Zondervan et al.,
226 2015), and results in improved long-term repeatability. Fractionation in the AMS system
227 may vary in sign depending on the particular conditions, but incomplete graphitization
228 biases the graphite towards lighter isotopes, which, if undiagnosed, will bias $\Delta^{14}\text{C}$ high.
229 The LG1 graphitisation system used during this period did not directly evaluate whether
230 graphitization was complete, so it is possible or even likely that there was a high bias in
231 the 1995 – 2005 measurements. This is further discussed in section 3.5.3.

232

233 For all EN Tandem samples, a single large aliquot of extracted CO_2 was split into four
234 separately graphitized and measured targets and the results of all four were averaged. We
235 have revisited the multi-target averaging, applying a consistent criterion to exclude
236 outliers and using a weighted mean of the retained measurements (supplementary
237 material). This results in differences of up to 5 ‰ relative to the values reported by
238 Currie et al. (2011) and is discussed in more detail in the supplementary material.

239

240 In 2010, the EN Tandem was replaced with a National Electrostatics Corporation AMS,
241 dubbed XCAMS (NZA > 34,000). XCAMS measures all three carbon isotopes, such that
242 the normalization correction is performed using the AMS measured ^{13}C values
243 (Zondervan et al., 2015). XCAMS measurements are made on single graphite targets
244 measured to high precision of typically 1.8 ‰ (Turnbull et al., 2015).

245

246 3.4. Results format

247 NaOH samples are collected over a period of typically two weeks, and sometimes much
248 longer. We report the date of collection as the average of the start and end dates. In
249 cases where the end date was not recorded, we use the start date. For a few samples, the
250 sampling dates were not recorded or are ambiguous, and those results have been excluded
251 from the reported dataset.

252

253 Results are reported here as $F^{14}\text{C}$ (Reimer et al., 2004) and $\Delta^{14}\text{C}$ (Turnbull et al., 2007).
254 $F^{14}\text{C}$ is corrected for isotopic fractionation and blank corrected. We calculated $F^{14}\text{C}$ from
255 the original measurement data recorded in our databases, and updated a handful of
256 records where transcription errors were found. $\Delta^{14}\text{C}$ is derived from $F^{14}\text{C}$, and corrected
257 for radioactive decay since the time of collection; this is slightly different from $\Delta^{14}\text{C}$ as
258 defined by Stuiver and Polach (1977) that is corrected to the date of measurement. $\Delta^{14}\text{C}$
259 has been recalculated using the date of collection for all results, resulting in changes of a
260 few tenths of permil in most $\Delta^{14}\text{C}$ values relative to those reported by Currie et al. (2011)
261 and Manning et al. (1990). Uncertainties are reported based on the counting statistical
262 uncertainty and for AMS measurements we add an additional error term, determined from
263 the long-term repeatability of secondary standard materials (Turnbull et al., 2015;
264 supplementary section 5.3). Samples for which changes have been made relative to the
265 previously published results are indicated by the quality flag provided in the

266 supplementary dataset. Where more than one measurement was made for a given date,
267 we report the weighted mean (Bevington and Robinson, 2003) of all measurements.
268

269 3.5. Smooth curve fits

270 In addition to the raw measured $\Delta^{14}\text{CO}_2$ values, we calculate a smooth curve fit and
271 deseasonalized trend from the Wellington $\Delta^{14}\text{C}$ and F^{14}C datasets. The deseasonalized
272 trend may be more useful than the raw data for aging of recent materials (e.g. Reimer et
273 al., 2004; Hua et al., 2013). Acknowledging that the 1995-2005 period is variable and
274 possibly biased in the Wellington record (section 4.3), we also provide in the
275 supplementary material an alternative mid-latitude Southern Hemisphere smooth curve fit
276 and deseasonalized trend in which the Wellington data for 1995-2005 has been removed
277 and replaced with the Cape Grim, Tasmania data for that period (Levin et al., 2010).
278

279 Curvefitting is particularly challenging for the $\Delta^{14}\text{CO}_2$ record, since (a) there are data
280 gaps and inconsistent sampling frequency, (b) the growth rate and trend vary dramatically
281 and (c) the seasonal cycle changes both in magnitude and phase (Section 5.2). We chose
282 to use the CCGCRV fitting procedure (Thoning et al., 1989;
283 www.esrl.noaa.gov/gmd/ccgg/mbl/crvfit/), which can readily handle the data gaps,
284 inconsistent sampling frequency, and rapid changes in the trend. To address the changing
285 seasonal cycle, we make separate fits to the record for five time periods: 1954-1965,
286 1966-1979, 1980-1989, 1990-2004, 2005-2014. These divisions were chosen based on
287 major changes in the raw observational growth rate, seasonal cycle and data quality
288 (supplementary section 6). For each time period, we use CCGCRV with one linear and
289 two harmonic terms and fit residuals are added back using a low-pass filter with an 80-
290 day cutoff in the frequency domain. At each transition, we overlapped a two-year period
291 and linearly interpolated the two fits across that two-year period to smooth the transitions
292 caused by end effects. The one-sigma uncertainty on the smoothed curve and
293 deseasonalized trend were determined using a Monte Carlo technique. Further details of
294 the fitting procedure and choice of time period cutoffs are provided in the supplementary
295 material.
296

297 The mean difference between the fitted curve and the measured $\Delta^{14}\text{CO}_2$ values is 3.8 ‰,
298 consistent with the typical measurement uncertainty for the full dataset. Further, the
299 residuals are highest for the early period (1954-1970) at 6 ‰, consistent with the larger
300 measurement errors at that time of ~6 ‰. The residuals improve as the measurement
301 errors reduce, such that since 2005, the mean residual is 2 ‰, consistent with the reported
302 2 ‰ uncertainties. The exception is the 1995- 2005 period where the mean residual
303 difference of 5 ‰ is substantially higher than the mean reported uncertainty of 2.5 ‰,
304 reflecting the apparent larger scatter during this period (Section 4.3).

305 4. Data validation

306 4.1. Tree ring comparison

307 Over the more than 60 years of the Wellington $\Delta^{14}\text{CO}_2$ record, there have necessarily
308 been many changes in methodology, and the tree rings provide a way to validate the full
309 record, albeit with lower resolution. Due to the possible sampling biases in the tree rings

310 (section 3.2.3.), we do not include them in the final updated record, but use them to
311 validate the existing measurements.

312

313 During the rapid $\Delta^{14}\text{CO}_2$ change in the early 1960s, there are some differences between
314 the kauri tree ring and Wellington $\Delta^{14}\text{CO}_2$ records (Figure 2). The 1963 and 1964 tree
315 ring samples are slightly lower than the concurrent $\Delta^{14}\text{CO}_2$ samples. The peak $\Delta^{14}\text{CO}_2$
316 measurement in the tree rings is 30 ‰ lower than the smoothed $\Delta^{14}\text{CO}_2$ record, and
317 100‰ lower than the two highest $\Delta^{14}\text{CO}_2$ measurements in 1965. These differences are
318 likely due to small errors in sampling of the rings, which will be most apparent during
319 periods of rapid change.

320

321 Prior to 1960 and from the peak of the bomb spike in 1965 until 1990, there is remarkable
322 agreement between the tree rings and Wellington $\Delta^{14}\text{CO}_2$ record, with the variability
323 replicated in both records. And since 2005, there is excellent agreement across all the
324 different records. Some differences are observed in 1990-1993 and 1995-2005, which we
325 discuss in the following sections.

326

327 4.2. 1990-1993 anomaly

328 An anomaly in the gas counting measurements between 1990 and 1993 has previously
329 been noted (figures 2, 3) as a deviation from the Cape Grim $\Delta^{14}\text{CO}_2$ record (CGO,
330 40.68°S, 144.68°E, 94 m asl, Levin et al., 2010) during the same period. Cape Grim is at
331 similar latitude, and observes a mixture of air from the mid-latitude Southern Ocean
332 sector and mainland Australia (Ziehn et al., 2014; Law et al., 2010). The Wellington and
333 Cape Grim records overlap during almost all other periods (figure 3).

334

335 We use archived CO_2 from flask samples to evaluate this period of deviation. First, the
336 recent flask samples collected since 2013 (n=12) agree very well with the NaOH static
337 samples from the same period (figure 2), indicating that despite the difference in
338 sampling period for the two methods, flask samples reflect the $\Delta^{14}\text{CO}_2$ observed in the
339 longer-term NaOH static samples. We then selected a subset of archived 1984 - 1992
340 extracted CO_2 samples for measurement, mostly from Southerly wind conditions, but
341 including a few from other wind conditions. These flask $\Delta^{14}\text{CO}_2$ measurements do not
342 exhibit the anomaly seen in the NaOH static samples (figure 2), implying that the
343 deviation observed in the original NaOH static samples may be a consequence of
344 sampling, storage or measurement errors. Annual tree rings from both the kauri and pine
345 follow the flask measurements for this period (figure 2), confirming that the NaOH static
346 samples are anomalous.

347

348 The 1990-1993 period was characterized by major changes in New Zealand science, both
349 in the organizational structure and personnel. Although we are unable to exactly
350 reconstruct events at that time, we hypothesize that the NaOH solution was prepared
351 slightly differently, perhaps omitting the barium chloride precipitation step for these
352 samples. This would result in contaminating CO_2 absorbed on the NaOH before the
353 solution was prepared. Since atmospheric $\Delta^{14}\text{CO}_2$ is declining, this would result in
354 higher $\Delta^{14}\text{CO}_2$ observed in these samples than in the ambient air. Another possibility is
355 that there were known issues with the background contamination in the proportional

356 counters during this period that could result in a high bias $\Delta^{14}\text{CO}_2$. In any case, these
357 values are anomalous and we remove the original NaOH static sample measurements
358 between 1990 and 1993 and replace them with the new flask measurements for the same
359 period.

360

361 4.3. 1995-2005 variability

362 As already discussed in section 3.3, the measurement method was changed from gas
363 counting to AMS for samples collected in 1995 and thereafter. During the first ten years
364 of AMS measurements, the record is much noisier than during any other period (figure
365 2). Until 2005, offline $\delta^{13}\text{C}$ measurements on the evolved CO_2 were used in the
366 normalization correction. In 2005, online ^{12}C measurement was added to the AMS
367 system, allowing online AMS measurement of the $\delta^{13}\text{C}$ value and accounting for any
368 fractionation during sample preparation and AMS measurement (Zondervan et al., 2015;
369 see also section 3.3). This substantially improved the measurement accuracy and the
370 noise in the $\Delta^{14}\text{CO}_2$ record immediately reduced as can be seen in the lower panel of
371 figure 2. Therefore, we suspect that the variability and apparent high bias in the 1995-
372 2005 period of the $\Delta^{14}\text{CO}_2$ record is due to measurement uncertainty and bias rather than
373 atmospheric variability.

374

375 The remaining NaOH solution for all samples collected since 1995 has been archived,
376 and typically only every second sample collected was measured, with the remainder
377 archived without extraction. In 2011-2016, we revisited the 1995-2005 period,
378 remeasuring some samples that had previously been measured and some that had never
379 been measured for a total of 52 new analyses.

380

381 The new measurements for this time period do show reduced scatter over the original
382 analyses, particularly for the period from 1998-2001 where the original analyses appear
383 anomalously low and in 2002-2003 when the original analyses appear anomalously high.
384 Yet there remain a number of both low and high outliers in the new measurements.
385 These are present in both the samples that were remeasured and in those for which this
386 was the first extraction of the sample. This suggests that a subset of the archived sample
387 bottles were either contaminated at the time of collection, or that some bottles were
388 insufficiently sealed, causing contamination with more recent CO_2 during storage.
389 Comparison with the tree ring measurements and with the Cape Grim record (Levin et al.,
390 2010) suggest that the measurements during this period may, on average, be biased high
391 as well as having additional scatter (figure 3). Nonetheless, in the absence of better data,
392 we retain both the original and remeasured NaOH sample results in the full Wellington
393 record, with a special flag to allow users to easily remove the questionable results if they
394 prefer. We also provide a smoothed fit that excludes these data (section 3.6).

395

396 5. Results and Discussion

397 5.1. Variability in the Wellington record through time

398 The Wellington $\Delta^{14}\text{CO}_2$ record begins in December 1954, at a roughly pre-industrial
399 $\Delta^{14}\text{CO}_2$ level of -20 ‰ (figure 2). From 1955, $\Delta^{14}\text{CO}_2$ increased rapidly, near doubling

400 to 700 ‰ in 1965 at Wellington, due to the production of ^{14}C during atmospheric nuclear
401 weapons tests. Nuclear tests in the early 1950s contributed to the rise, then a hiatus in
402 testing in the late 1950s led to a plateau in Wellington $\Delta^{14}\text{CO}_2$ before a series of very
403 large atmospheric tests in the early 1960s led to further increases (Rafter and Ferguson,
404 1959; Manning et al., 1990).

405
406 Most atmospheric nuclear weapons testing ceased in 1963, and the Wellington $\Delta^{14}\text{CO}_2$
407 record peaks in 1965 then begins to decline, at first rapidly at -30 ‰ yr^{-1} in the 1970s and
408 gradually slowing to -5 ‰ yr^{-1} after 2005. The initial rapid decline has been attributed
409 primarily to the uptake of the excess radiocarbon into the oceans, and to a lesser extent,
410 uptake into the terrestrial biosphere (Naegler et al 2006; Randerson et al., 2002; Manning
411 et al., 1990; Stuiver and Quay 1981). The short residence time of carbon in the biosphere
412 means that from the 1980s, the terrestrial biosphere changed from a ^{14}C sink to a ^{14}C
413 source as the bomb pulse was re-released (Randerson et al., 2002; Levin et al., 2010).

414
415 Natural cosmogenic production of ^{14}C damps the rate of decline since the bomb peak by
416 $\sim 5 \text{ ‰ yr}^{-1}$ in $\Delta^{14}\text{CO}_2$; this may vary with the solar cycle, but there is no known long-term
417 trend in this component of the signal (Turnbull et al., 2009; Naegler et al., 2006). There
418 is also a small positive contribution from the nuclear industry which emits ^{14}C to the
419 atmosphere, and this has increased from zero in the 1950s to $0.5 - 1 \text{ ‰ yr}^{-1}$ in the last
420 decade (Turnbull et al., 2009b; Levin et al., 2010; Graven and Gruber, 2011).

421
422 The Suess Effect, the decrease in atmospheric $\Delta^{14}\text{CO}_2$ due to the addition of ^{14}C -free
423 fossil fuel CO_2 to the atmosphere (Suess, 1955; Tans, 1979; Levin et al., 2003), was first
424 recognized in 1955 and has played a role throughout the record. Although the magnitude
425 of fossil fuel CO_2 emissions has grown through time, when convolved with the declining
426 atmospheric $\Delta^{14}\text{CO}_2$ history, the impact on $\Delta^{14}\text{CO}_2$ stayed roughly constant at -10 ‰ yr^{-1}
427 from the 1970s to the mid-2000s (Randerson et al., 2002; Levin et al., 2010; Graven et
428 al., 2012). Yet the continued increase in fossil fuel CO_2 emissions has slightly increased
429 the impact of fossil fuel CO_2 in the last few years, to about -12 ‰ yr^{-1} in 2014 (using
430 annual global fossil fuel CO_2 estimates from CDIAC (Boden et al., 2017)). Since the
431 1990s, the Suess Effect has been the largest driver of the ongoing negative growth rate
432 (Turnbull et al., 2009b; Levin et al., 2010).

433
434 The most recent part of the Wellington $\Delta^{14}\text{CO}_2$ record from 2005 – 2014 is reported here
435 for the first time. It shows a continuing downward trend in $\Delta^{14}\text{CO}_2$ of -5 ‰ yr^{-1} , a slight
436 slowing in the negative trend relative to the 1990 – 2004 period which had a trend of
437 5.8 ‰ yr^{-1} . This slight slowing in the downward $\Delta^{14}\text{CO}_2$ trend is opposite of what might
438 be expected due to the Suess Effect alone. Possible explanations are a slowing of the rate
439 of uptake of ^{14}C into the oceans, an increase in the return rate of bomb ^{14}C to the
440 atmosphere from the biosphere, and a secular increase in ^{14}C production.

441

442 5.2 Seasonal variability in the Wellington record

443 We determine the changing seasonal cycle from smooth curve fits to five separate periods
444 of the record (1954-1965, 1966-1979, 1980-1989, 1990-2004, 2005-2014, figure 4 top
445 panel). This subdivision is necessary to allow the seasonal cycle to vary through time

446 since the CCGCRV curve fitting routine assigns a single set of harmonics to the time
447 period fitted (see section 3.5). The choice of time periods is discussed in supplementary
448 section 6. We also created detrended, fitted $\Delta^{14}\text{CO}_2$ seasonal cycles by subtracting the
449 deseasonalised trend from the observations. Comparison with the detrended, fitted
450 seasonal cycle determined from the smooth curve fits (figure 4 bottom panel) shows that
451 the smooth curve fit, as might be expected, does not capture the largest deviations from
452 the trend seen in the observations, but represents the changing seasonal cycle quite well.

453

454 The 1966-1979 period shows a strong seasonal cycle (figure 4) with a consistent phase
455 and an amplitude that varies from a maximum in 1966 of 30‰ gradually declining to
456 3 ‰ in 1979, with a mean amplitude of about 6 ‰. This is primarily attributed to
457 seasonally varying stratosphere – troposphere exchange bringing bomb ^{14}C into the
458 troposphere (Manning et al., 1990; Randerson et al., 2002). Manning et al. (1990) were
459 unable to simulate the correct phasing of the seasonal cycle, apparently because their
460 model distributed bomb ^{14}C production throughout both Northern and Southern
461 stratosphere. In fact, the majority of the bomb ^{14}C was produced in the Northern
462 Hemisphere stratosphere (Enting et al., 1982). Randerson et al (2002) were able to match
463 the amplitude of the Wellington seasonal cycle during this time period, although their
464 model was out of phase with the observations by about 1.5 months. They attribute the
465 seasonal cycle during this period mostly to the seasonality in Northern Hemisphere
466 stratosphere – troposphere exchange with a phase lag caused by cross-equator exchange
467 into the Southern Hemisphere. The seasonal cycle kept the same phase but gradually
468 decreased in amplitude until the late 1970s, attributed to the declining disequilibrium
469 between the stratosphere and troposphere as the bomb ^{14}C moved throughout the carbon
470 reservoirs.

471

472 Between 1978 and 1980 the seasonal cycle weakened, and then reversed during the
473 1980s, with a maximum in winter (June – August) and amplitude of about 2 ‰. The
474 detrended observations show that this change in phase is not an artifact of the fitting
475 method (bottom panel of figure 4). This result is comparable to that obtained by
476 Manning et al. (1990) and Currie et al. (2011), who both used a seasonal trend loess
477 (STL) procedure to determine the seasonal cycle from the same data. This is consistent
478 with the seasonality in atmospheric transport convolving with a change in sign of the
479 terrestrial biosphere contribution as the bomb ^{14}C pulse began to return to the atmosphere
480 from the biosphere (Randerson et al., 2002).

481

482 The Wellington $\Delta^{14}\text{CO}_2$ seasonal cycle declined in the 1990s, and the larger variability in
483 the observations between 1995 and 2005 makes it difficult to discern a seasonal cycle
484 during that period. Since 2005, the more precise measurements allow us to detect a small
485 seasonal cycle with amplitude of about 2 ‰ (figure 4). We compare the seasonal cycle at
486 Wellington from 2005 – 2015 with the seasonal cycle at Cape Grim, Australia from 1995-
487 2010. There is no significant difference in the seasonal cycle at either site if we select
488 only the overlapping time period of 2005-2010. Both sites show a similar magnitude
489 seasonal cycle during this period, and Cape Grim shows a maximum in March – April
490 that has been attributed primarily to the seasonality of atmospheric transport of Northern
491 Hemisphere fossil fuel emissions to the Southern troposphere (Levin et al., 2010). This

492 maxima at Cape Grim coincides with a seasonal maximum in the Wellington record.
493 However, Wellington $\Delta^{14}\text{CO}_2$ exhibits a second maximum in the austral spring (October)
494 that is not apparent at Cape Grim.

495
496 Recent work has shown that during the winter, the Cape Grim station is influenced by air
497 coming off the Australian mainland including the city of Melbourne (Ziehn et al., 2014),
498 which would act to reduce $\Delta^{14}\text{CO}_2$ at Cape Grim relative to Southern Ocean clean air.
499 This shift is shown to be the result of seasonal variations in atmospheric transport. The
500 two-week integrated sampling used for $\Delta^{14}\text{CO}_2$ at both Cape Grim and Baring Head
501 means that in contrast to other species, $\Delta^{14}\text{CO}_2$ measurements cannot be screened to
502 remove these pollution events.

503
504 In contrast, the Baring Head location near Wellington does not show significant seasonal
505 variation in atmospheric transport (Steinkamp et al., 2017) and Baring Head is less likely
506 than Cape Grim to be influenced by anthropogenic emissions in any season. Air is
507 typically from the ocean, and the local geography means that the urban emission plume
508 from Wellington and its northern suburbs of Lower Hutt very rarely passes over Baring
509 Head (figure 1) and the typically high wind speeds further reduce the influence of the
510 local urban area (Stephens et al., 2013). During the austral autumn, there is some land
511 influence from the Christchurch region in the South Island, but emissions from
512 Christchurch are much smaller than the Melbourne emissions influencing Cape Grim:
513 State of Victoria fossil fuel CO_2 emissions for 2013 were 23 MtC whereas Wellington
514 and Christchurch each emitted 0.4 MtC of fossil fuel CO_2 in 2013 (Boden et al., 2017;
515 AECOM, 2016; Australian Government, 2016).

516
517 Although broad-scale flow from the west is common, the local topography means that
518 local air flow is almost always either southerly or northerly (Stephens et al., 2013), but
519 during rare (<5% of the time) westerly wind events, fossil fuel emissions from
520 Wellington do appear to cause enhancements of up to 2 ppm in CO_2 (Stephens et al.,
521 2013), which would decrease $\Delta^{14}\text{CO}_2$ by ~ 1 ‰ during such an event. Yet there is no
522 evidence of seasonality in the infrequent westerly events. Northerly conditions bring a
523 terrestrial biosphere influence that elevates CO_2 by about 1 ppm (Stephens et al., 2013),
524 which could result in a maximum increase in $\Delta^{14}\text{CO}_2$ of ~ 0.2 ‰ relative to background
525 conditions, but there is no evidence that this influence is seasonally variable either. Thus,
526 although there are some local influences on the Baring Head $\Delta^{14}\text{CO}_2$, none of these
527 appear to be seasonally dependent and instead, the observed Baring Head $\Delta^{14}\text{CO}_2$
528 maximum in spring in the recent part of the record may be explained by the seasonal
529 maximum in cross-tropopause exchange bringing ^{14}C -enriched air at this time of year.

530

531 5.3. Comparison with other atmospheric $\Delta^{14}\text{CO}_2$ records

532 We compare the Wellington $\Delta^{14}\text{CO}_2$ record with several other $\Delta^{14}\text{CO}_2$ records, located as
533 indicated in figure 1. First, we compare with measurements from Cape Grim, Australia
534 (CGO, 40.68°S, 144.68°E, 94 m asl). Cape Grim is at similar latitude to Wellington and
535 also frequently receives air from the Southern Ocean (Levin et al., 2010). Samples are
536 collected by a similar method to the Wellington record using NaOH absorption and are
537 measured by gas counting to ~ 2 ‰ precision. Next, we compare with mid-latitude high-

538 altitude clean air sites in the Northern Hemisphere. The Vermont, Austria (VER,
539 47.07°N, 9.57°E, 1800 m asl) record began in 1958, only a few years after the Wellington
540 record began, and in the 1980s the site was moved to Jungfrauoch, Switzerland (JFJ,
541 46.55°N, 7.98°E, 3450 m asl); these measurements are made in the same manner and by
542 the same laboratory as the Cape Grim record (Levin et al., 2013). We also consider the
543 Niwot Ridge, USA $\Delta^{14}\text{CO}_2$ record (NWR, 40.05°N, 105.59°W, 3523 m asl), which began
544 in 2003 (Turnbull et al., 2007; Lehman et al., 2013). Niwot Ridge is also a mid-latitude
545 high-altitude site, but samples are collected as whole air in flasks and measured by AMS
546 in a similar manner to that described for the Wellington flask samples. Thus, we are
547 comparing two independent Southern Hemisphere records with two independent
548 Northern Hemisphere records, with the two hemispheres tied together by the common
549 measurement laboratory used for Cape Grim and Jungfrauoch. Results from all records
550 are compared in figure 5.

551

552 The Wellington and Cape Grim records are generally consistent with one another (Figure
553 3), with the exception of the 1995-2005 period, when the Wellington record is slightly
554 higher, apparently due to bias in the Wellington record (discussed in section 3.5.3.).
555 Differences between the sites are smaller than the measurement uncertainty for all other
556 periods (table 2). This implies that $\Delta^{14}\text{CO}_2$ is homogeneous across Southern Hemisphere
557 clean air sites within the same latitude band, at least since the 1980s when the two records
558 overlap. Similarly, the high altitude, mid-latitude Northern Hemisphere sites are
559 consistent with one another, although there are some differences in seasonal cycles in
560 recent years (Turnbull et al., 2009b).

561

562 The bomb spike maximum is higher and earlier in the Northern Hemisphere records
563 (figure 5), consistent with the production of most bomb ^{14}C in the Northern Hemisphere
564 stratosphere. We make a new, simple estimate of the interhemispheric exchange time
565 during the 1963 – 1965 period using the difference in the timing of the Northern and
566 Southern Hemisphere bomb peaks. The first maximum of the bomb peak was in July
567 1963 in the Northern Hemisphere and January 1965 in the Southern Hemisphere, a 1.4
568 year offset, implying a 1.4 year exchange time. This is consistent with other more
569 detailed interhemispheric exchange time estimates that have been determined from long-
570 term measurements of SF_6 of 1.3 to 1.4 years (Geller et al., 1997; Patra et al., 2011).

571

572 Northern Hemisphere $\Delta^{14}\text{CO}_2$ remains higher than Southern Hemisphere $\Delta^{14}\text{CO}_2$ by
573 about 20 ‰ until 1972. Although most nuclear weapons testing ceased in 1963, a few
574 smaller tests continued in the late 1960s, contributing to this continued interhemispheric
575 offset (Enting, 1982). The interhemispheric gradient disappeared within about 1.5 years
576 after atmospheric testing essentially stopped in 1970. Except periods of noisy data from
577 Vermont in the late 1970s and Wellington in 1995-2005, there are only small (<2 ‰)
578 interhemispheric gradients from 1972 until 2002 (figure 5, table 2).

579

580 As previously noted by Levin et al. (2010) using a shorter dataset, an interhemispheric
581 gradient of 5-7 ‰ develops in 2002, with the Southern Hemisphere sites higher than the
582 Northern Hemisphere sites (table 2). We choose 1986 – 1990 and 2005 – 2013 as time
583 periods to compare, to avoid the periods where the Wellington record is noisy (1995 –

584 2005) and where we substituted flask measurements from 1990 – 1993. In 1986 – 1990,
585 there is less than 2 ‰ difference between Wellington and either Cape Grim or
586 Jungfraujoch. There is also no difference between the Cape Grim and Jungfraujoch
587 records during this time period. The Wellington and Cape Grim records still agree
588 within 2 ‰ after 2005, but both Jungfraujoch and Niwot Ridge diverge from Wellington,
589 by 4.8 ± 2.7 and 6.9 ± 2.5 ‰, respectively; Jungfraujoch and Niwot Ridge are not
590 significantly different from one another. This new interhemispheric gradient is robust,
591 being consistent amongst the sites measured by three different research groups each with
592 their own methods. It is not an artifact of interlaboratory offsets, since Cape Grim and
593 Jungfraujoch measurements are made by the same group using the same sampling and
594 measurement methods, and the Wellington and Niwot Ridge measurements (measured by
595 different techniques) agree well with the other sites at similar latitude (Cape Grim and
596 Jungfraujoch respectively). This developing gradient is also apparent in the larger
597 sampling network of Levin et al (2010) and in a separate $\Delta^{14}\text{CO}_2$ sampling network
598 (Graven et al., 2012), although that dataset extends only to 2007.

599
600 Graven et al. (2012) demonstrated that increasing (mostly Northern Hemisphere) fossil
601 fuel CO_2 emissions cannot explain this $\Delta^{14}\text{CO}_2$ interhemispheric gradient, and instead,
602 they postulated that ^{14}C uptake into the Southern Ocean reduced over time. Levin et al.
603 (2010) were able to roughly replicate this interhemispheric gradient in their GRACE
604 model by tuning the terrestrial biosphere fluxes to match the observed global average
605 atmospheric CO_2 and $\Delta^{14}\text{CO}_2$ records. Where the observations suggest the rapid
606 development of an interhemispheric gradient in the early 2000's (figure 5), the GRACE
607 model simulates a more gradual transition over a period of roughly two decades.
608 Independent evidence suggests that the Southern Ocean is more likely to be responsible
609 for this rapid shift in the atmospheric $\Delta^{14}\text{CO}_2$ gradient. That is, an apparent
610 reorganization of Southern Ocean carbon exchange in the early 2000s (Landschützer et
611 al., 2015) is postulated to be associated with changes in upwelling of deep water
612 (DeVries et al., 2017), to which atmospheric $\Delta^{14}\text{CO}_2$ is highly sensitive (Rodgers et al.,
613 2011; Graven et al., 2012b). The observed $\Delta^{14}\text{CO}_2$ interhemispheric gradient is
614 consistent with these postulated changes in upwelling. Other possible explanations for
615 this new interhemispheric $\Delta^{14}\text{CO}_2$ gradient are substantial underreporting of Northern
616 Hemisphere fossil CO_2 emissions (e.g. Francey et al., 2013) or changes in the land carbon
617 sink (Wang et al., 2013; Sitch et al., 2015), although this latter is less likely since $\Delta^{14}\text{CO}_2$
618 is much less sensitive to biospheric fluxes than to either ocean or fossil fuel fluxes (e.g.
619 Levin et al., 2010; Turnbull et al., 2009). Given the limited spatial coverage of the current
620 $\Delta^{14}\text{CO}_2$ observing network, it is not possible to robustly determine which of these
621 processes causes the interhemispheric gradient. This could be achieved with more
622 observations of the spatial and temporal variations of atmospheric $\Delta^{14}\text{CO}_2$.

623 6. Conclusions

624 The 60 year-long Wellington $\Delta^{14}\text{CO}_2$ record has been revised and extended to 2014.
625 Most revisions were minor, but we particularly note that the earlier reported 1990-1993
626 measurements have been entirely replaced with new measurements. A second period
627 from 1995-2005 has poorer data quality than the rest of the record, and may also be
628 biased high by a few permil. These data have been revised substantially, and new

629 measurements have been added to this period, but we were unable to definitively identify
630 or correct for bias, so the data have been retained, albeit with caution. We further
631 validated the record by comparison with tree ring samples collected from the Baring
632 Head sampling location and from nearby Eastbourne, Wellington; both tree ring records
633 show excellent agreement with the original record, and indicate that there are no other
634 periods where the original measurements are problematic.

635

636 The Wellington $\Delta^{14}\text{CO}_2$ time series records the history of atmospheric nuclear weapons
637 testing and the subsequent decline of $\Delta^{14}\text{CO}_2$ as the bomb ^{14}C moved throughout the
638 carbon cycle, and ^{14}C -free fossil fuel emissions further decreased $\Delta^{14}\text{CO}_2$. The timing of
639 the first appearance of the bomb- ^{14}C peak at Wellington is consistent with other recent
640 estimates of interhemispheric exchange time at 1.4 years.

641

642 The seasonal cycle at Wellington evolves through the record, apparently dominated by
643 the seasonality of cross-tropopause transport, which drives a changing seasonal cycle
644 through time. In the early post-bomb period, the seasonally variable movement of bomb
645 ^{14}C from the Northern Stratosphere through the Northern Troposphere to the Southern
646 Troposphere appears to be the dominant control on the seasonal cycle at Wellington. The
647 seasonal cycle reversed in later years, possibly due to a change in sign of the terrestrial
648 biosphere $\Delta^{14}\text{C}$ signal. In recent years, the seasonal cycle has an amplitude of only 2 ‰,
649 with a maximum in the austral spring. Cape Grim exhibits a similar seasonal cycle
650 magnitude, but appears to be very slightly influenced by a terrestrial/anthropogenic signal
651 during the austral winter that is not apparent at Wellington.

652

653 During the 1980s and 1990s, $\Delta^{14}\text{CO}_2$ was similar at mid-latitude clean air sites in both
654 hemispheres, but since the early 2000s, the Northern Hemisphere $\Delta^{14}\text{CO}_2$ has dropped
655 below the Southern Hemisphere by 5-7 ‰. The control on this changing
656 interhemispheric gradient cannot be robustly determined from the existing sparse $\Delta^{14}\text{CO}_2$
657 observations, but may be due to a change in Southern Ocean dynamics reducing
658 upwelling of old, ^{14}C -poor deep waters, consistent with recent evidence for an increasing
659 Southern Ocean carbon sink. Alternative explanations are an underestimate of Northern
660 Hemisphere fossil fuel CO_2 emissions, or a changing land carbon sink. This implies that
661 ongoing and expanded Southern Hemisphere $\Delta^{14}\text{CO}_2$ observations and modelling may
662 provide a fundamental constraint on our understanding of Southern Ocean dynamics and
663 exchange processes.

664 7. Acknowledgements

665 A 60 year-long record takes more than a handful of authors to produce. This work was
666 possible only because of the amazing foresight and scientific understanding of Athol
667 Rafter and Gordon Fergusson, who began this record in the 1950s. Their work was
668 continued over the years by a number of people, including Hugh Melhuish, Martin
669 Manning, Dave Lowe, Rodger Sparks, Charlie McGill, Max Burr and Graeme Lyon.
670 This work was funded by the Government of New Zealand as GNS Science Global
671 Change Through Time core funding and NIWA Greenhouse Gases, Emissions, and
672 Carbon Cycle Science Programme core funding. The author(s) wish to acknowledge the
673 contribution of New Zealand eScience Infrastructure (NeSI) to the results of this research.

674 New Zealand's national computer and analytics services and team are supported by the
675 NeSI and funded jointly by NeSI's collaborator institutions and through the Ministry of
676 Business, Innovation and Employment (<http://www.nesi.org.nz>). We thank Dr Scott
677 Lehman (University of Colorado) and Dr Ingeborg Levin (University of Heidelberg) for
678 sharing their $\Delta^{14}\text{CO}_2$ datasets for comparison with the Wellington record.
679

680 8. Data availability

681 The datasets presented in this paper are included as supplementary material. The datasets
682 (including updates as they are available) can be accessed through the World Data Centre
683 for Greenhouse Gases (<http://ds.data.jma.go.jp/gmd/wdcgg/>) or directly through GNS
684 Science ([https://gns.cri.nz/Home/Products/Databases/Wellington-atmospheric-14CO2-](https://gns.cri.nz/Home/Products/Databases/Wellington-atmospheric-14CO2-record)
685 [record](https://gns.cri.nz/Home/Products/Databases/Wellington-atmospheric-14CO2-record)) or NIWA (<ftp://ftp.niwa.co.nz/tropac/>).

686 9. References

- 687 AECOM New Zealand Limited, 2016. Community greenhouse gas inventory for
688 Wellington City and the Greater Wellington Region 2000-2015, Wellington.
- 689 Australian Government, 2016. State and territory greenhouse gas inventories 2014.
690 Department of the Environment.
- 691 Baisden, W.T., Prior, C.A., Chambers, D., Canessa, S., Phillips, A., Bertrand, C.,
692 Zondervan, A., Turnbull, J.C., 2013. Radiocarbon sample preparation and data flow
693 at Rafter: Accommodating enhanced throughput and precision. *Nuclear Instruments
694 and Methods B294*, 194-198.
- 695 Bevington, P.R., Robinson, D.K., 2003. Data reduction and error analysis for the physical
696 sciences, Third Edition. McGraw-Hill.
- 697 Boden, T.A., Marland, G., Andres, R.J., 2017. Global, Regional, and National Fossil-Fuel
698 CO₂ Emissions. Carbon Dioxide Information Analysis Center, Oak Ridge National
699 Laboratory, U.S. Department of Energy, Oak Ridge, Tenn., U.S.A.
- 700 Bozhinova, D., Combe, M., Palstra, S.W.L., Meijer, H.A.J., Krol, M.C., Peters, W., 2013.
701 The importance of crop growth modeling to interpret the ¹⁴CO₂ signature of annual
702 plants. *Global Biogeochemical Cycles* 27, 792-803.
- 703 Brailsford, G.W., Stephens, B.B., Gomez, A.J., Riedel, K., Mikaloff Fletcher, S.E.,
704 Nichol, S.E., Manning, M.R., 2012. Long-term continuous atmospheric CO₂
705 measurements at Baring Head, New Zealand. *Atmospheric Measurement
706 Techniques* 5, 3109-3117.
- 707 Broecker, W.S., Peng, T.-H., Ostlund, H., Stuiver, M., 1985. The distribution of bomb
708 radiocarbon in the ocean. *Journal of Geophysical Research* C4, 6953-6970.
- 709 Caldeira, K., Rau, G.H., Duffy, P.B., 1998. Predicted net efflux of radiocarbon from the
710 ocean and increase in atmospheric radiocarbon content. *Geophysical Research
711 Letters* 25, 3811-3814.
- 712 Cleveland, R., Cleveland, W., McRae, J., Terpenning, I., 1990. STL: A seasonal-trend
713 decomposition procedure based on Loess. *Journal of Official Statistics* 6, 3-33.
- 714 Currie, K.I., Brailsford, G., Nichol, S., Gomez, A., Sparks, R., Lassey, K.R., Riedel, K.,
715 2011. Tropospheric ¹⁴CO₂ at Wellington, New Zealand: the world's longest record.
716 *Biogeochemistry* 104, 5-22.
- 717 Davies, T., Cullen, M., Malcolm, A., Mawson, M., Staniforth, A., White, A., Wood, N.,
718 2005. A new dynamical core for the Met Office's global and regional modelling of
719 the atmosphere. *Quarterly Journal of the Royal Meteorological Society* 131, 1759-
720 2005.
- 721 DeVries, T., Holzer, M., Primeau, F., 2017. Recent increase in oceanic carbon uptake
722 driven by weaker upper-ocean overturning. *Nature* 542, 215-218.
- 723 Djuricin, S., Pataki, D.E., Xu, X., 2010. A comparison of tracer methods for quantifying
724 CO₂ sources in an urban region. *Journal of Geophysical Research* 115.
- 725 Enting, I.G., 1982. Nuclear weapons data for use in carbon cycle modelling. CSIRO
726 Division of Atmospheric Physics and Technology, Melbourne, Australia.
- 727 Ferretti, D.F., Lowe, D.C., Martin, R.H., Brailsford, G.W., 2000. A new gas
728 chromatograph-isotope ratio mass spectrometry technique for high-precision, N₂O-
729 free analysis of δ¹³C and δ¹⁸O in atmospheric CO₂ from small air samples. *Journal
730 of Geophysical Research Atmospheres* 105, 6709-6718.

731 Francey, R.J., Trudinger, C.M., van der Schoot, M., Law, R.M., Krummel, P.B.,
732 Langenfelds, R.L., Steele, L.P., Allison, C.E., Stavert, A.R., Andres, R.J.,
733 Rödenbeck, C., 2013. Atmospheric verification of anthropogenic CO₂ emission
734 trends. *Nature Climate Change* 3, 520-524.

735 Geller, L.S., Elkins, J.W., Lobert, J.M., Clarke, A.D., Hurst, D.F., Butler, J.H., Myers,
736 R.C., 1997. Tropospheric SF₆: Observed latitudinal distribution and trends, derived
737 emissions and interhemispheric exchange time. *Geophysical Research Letters* 24,
738 675-678.

739 Graven, H.D., Gruber, N., 2011. Continental-scale enrichment of atmospheric ¹⁴CO₂ from
740 the nuclear power industry: potential impact on the estimation of fossil fuel-derived
741 CO₂. *Atmospheric Chemistry and Physics* 11, 12339-12349.

742 Graven, H.D., Guilderson, T.P., Keeling, R.F., 2012. Observations of radiocarbon in CO₂
743 at seven global sampling sites in the Scripps flask network: Analysis of spatial
744 gradients and seasonal cycles. *Journal of Geophysical Research* 117.

745 Hogg, A.G., 2013. SHCAL13 Southern Hemisphere calibration, 0-50,000 years CAL BP.
746 Radiocarbon.

747 Hua, Q., Barbetti, M., Jacobsen, G., Zoppi, U., Lawson, E., 2000. Bomb radiocarbon in
748 annual tree rings from Thailand and Australia. *Nuc. Inst. and Meth. in Physics*
749 *Research B* 172, 359-365.

750 Hua, Q., Barbetti, M., Rakowski, A.Z., 2013. Atmospheric radiocarbon for the period
751 1950-2010. *Radiocarbon* 55, 1-14.

752 Jones, A.R., Thomson, D., Hort, M., Devenish, B., 2007. The UK Met Office's next-
753 generation atmospheric dispersion model, NAME III, in: Borrego, C., Norman, A.-
754 L. (Eds.), *Air Pollution Modeling and Its Application XVII*. Springer.

755 Kanu, A., Comfort, L., Guilderson, T.P., Cameron-Smith, P.J., Bergmann, D.J., Atlas,
756 E.L., Schauffler, S., Boering, K.A., 2015. Measurements and modelling of
757 contemporary radiocarbon in the stratosphere. *Geophysical Research Letters* 43.

758 Keeling, C.D., Piper, S.C., Whorf, T.P., Keeling, R.F., 2011. Evolution of natural and
759 anthropogenic fluxes of atmospheric CO₂ from 1957 to 2003. *Tellus B* 63, 1-22.

760 Keeling, C.D., Whorf, T., 2005. Atmospheric CO₂ records from sites in the SIO air
761 sampling network, *Trends: A compendium of data of global change*. Carbon
762 Dioxide Information Analysis Center, Oak Ridge National Laboratory, Oak Ridge,
763 Tenn., USA.

764 Key, R.M., 2004. A global ocean carbon climatology: Results from Global Data Analysis
765 Project (GLODAP). *Global Biogeochemical Cycles* 18.

766 Kjellström, E., Feichter, J., Hoffman, G., 2000. Transport of SF₆ and ¹⁴CO₂ in the
767 atmospheric general circulation model ECHAM4. *Tellus* 52B, 1-18.

768 Landschützer, P., Gruber, N., Haumann, F.A., Rödenbeck, C., Bakker, D.C.E., van
769 Heuven, S., Hoppema, M., Metzl, N., Sweeney, C., Takahashi, T., Tilbrook, B.,
770 Wanninkhof, R., 2015. The reinvigoration of the Southern Ocean carbon sink.
771 *Science* 349, 1221-1224.

772 Law, R.M., Steele, L.P., Krummel, P.B., Zahorowski, W., 2010. Synoptic variations in
773 atmospheric CO₂ at Cape Grim: a model intercomparison. *Tellus B* 62, 810-820.

774 Le Quere, C., Rodenbeck, C., Buitenhuis, E.T., Conway, T.J., Langenfelds, R., Gomez,
775 A., Labuschagne, C., Ramonet, M., Nakazawa, T., Metzl, N., Gillett, N., Heimann,

776 M., 2007. Saturation of the Southern Ocean CO₂ Sink Due to Recent Climate
777 Change. *Science* 316, 1735-1738.

778 Lehman, S.J., Miller, J.B., Wolak, C., Southon, J.R., Tans, P.P., Montzka, S.A., Sweeney,
779 C., Andrews, A.E., LaFranchi, B.W., Guilderson, T.P., Turnbull, J.C., 2013.
780 Allocation of terrestrial carbon sources using ¹⁴CO₂: Methods, measurement, and
781 modelling. *Radiocarbon* 55, 1484-1495.

782 Levin, I., Kromer, B., Hammer, S., 2013. Atmospheric Δ¹⁴CO₂ trend in Western
783 European background air from 2000 to 2012. *Tellus B* 65.

784 Levin, I., Kromer, B., Schmidt, M., Sartorius, H., 2003. A novel approach for
785 independent budgeting of fossil fuel CO₂ over Europe by ¹⁴CO₂ observations.
786 *Geophysical Research Letters* 30, 2194.

787 Levin, I., Kromer, B., Schoch-Fischer, H., Bruns, M., Munnich, M., Berdau, D., Vogel,
788 J.C., Munnich, K.O., 1985. 25 years of tropospheric ¹⁴C observations in central
789 Europe. *Radiocarbon* 27, 1-19.

790 Levin, I., Naegler, T., Kromer, B., Diehl, M., Francey, R.J., Gomez-Pelaez, A.J., Steele,
791 L.P., Wagenbach, D., Weller, R., Worthy, D.E., 2010. Observations and modelling
792 of the global distribution and long-term trend of atmospheric ¹⁴CO₂. *Tellus B* 62,
793 26-46.

794 Lopez, M., Schmidt, M., Delmotte, M., Colomb, A., Gros, V., Janssen, C., Lehman, S.J.,
795 Mondelain, D., Perrussel, O., Ramonet, M., Xueref-Remy, I., Bousquet, P., 2013.
796 CO, NO_x and ¹³CO₂ as tracers for fossil fuel CO₂: results from a pilot study in Paris
797 during winter 2010. *Atmospheric Chemistry and Physics* 13, 7343-7358.

798 Lowe, D.C., Judd, W., 1987. Graphite target preparation for radiocarbon dating by
799 accelerator mass spectrometry. *Nuclear Instruments and Methods in Physics*
800 *Research B* 28, 113-116.

801 Manning, M.R., Lowe, D.C., Melhuish, W.H., Sparks, R.J., Wallace, G., Brenninkmeijer,
802 C.A.M., McGill, R.C., 1990. The use of radiocarbon measurements in atmospheric
803 sciences. *Radiocarbon* 32, 37-58.

804 Meijer, H.A.J., Pertuisot, M.-H., van der Plicht, J., 2006. High accuracy ¹⁴C
805 measurements for atmospheric CO₂ samples by AMS. *Radiocarbon* 48, 355-372.

806 Meijer, H.A.J., Smid, H.M., Perez, E., Keizer, M.G., 1996. Isotopic characterization of
807 anthropogenic CO₂ emissions using isotopic and radiocarbon analysis. *Physical*
808 *Chemistry of the Earth* 21, 483-487.

809 Miller, J.B., Lehman, S.J., Montzka, S.A., Sweeney, C., Miller, B.R., Wolak, C.,
810 Dlugokencky, E.J., Southon, J.R., Turnbull, J.C., Tans, P.P., 2012. Linking
811 emissions of fossil fuel CO₂ and other anthropogenic trace gases using atmospheric
812 ¹⁴CO₂. *Journal of Geophysical Research* 117, D08302.

813 Munro, D.R., Lovenduski, N.S., Takahashi, T., Stephens, B.B., Newberger, T., Sweeney,
814 C., 2015. Recent evidence for a strengthening CO₂sink in the Southern Ocean from
815 carbonate system measurements in the Drake Passage (2002-2015). *Geophysical*
816 *Research Letters*, n/a-n/a.

817 Naegler, T., Ciais, P., Rodgers, K., Levin, I., 2006. Excess radiocarbon constraints on air-
818 sea gas exchange and the uptake of CO₂ by the oceans. *Geophysical Research*
819 *Letters* 33.

820 Naegler, T., Levin, I., 2009. Observation-based global biospheric excess radiocarbon
821 inventory 1963–2005. *Journal of Geophysical Research* 114.

822 Norris, M.W., 2015. Reconstruction of historic fossil CO₂ emissions using radiocarbon
823 measurements from tree rings, School of Geography, Environment and Earth
824 Sciences. Victoria University of Wellington.

825 Nydal, R., Lövseth, K., 1983. Tracing bomb ¹⁴C in the atmosphere 1962-1980. *Journal of*
826 *Geophysical Research* 88, 3621-3642.

827 Oeschger, H., Siegenthaler, U., Schotterer, U., Gugelmann, A., 1975. A box diffusion
828 model to study the carbon dioxide exchange in nature. *Tellus XXVII*, 168-192.

829 Otago Daily Times, 1957. Polar ice caps may melt with industrialisation, Otago Daily
830 Times, 23/1/1957 ed, Dunedin, New Zealand, p. 1.

831 Patra, P.K., Houweling, S., Krol, M., Bousquet, P., Belikov, D., Bergmann, D., Bian, H.,
832 Cameron-Smith, P., Chipperfield, M.P., Corbin, K., Fortems-Cheiney, A., Fraser,
833 A., Gloor, E., Hess, P., Ito, A., Kawa, S.R., Law, R.M., Loh, Z., Maksyutov, S.,
834 Meng, L., Palmer, P.I., Prinn, R.G., Rigby, M., Saito, R., Wilson, C., 2011.
835 TransCom model simulations of CH₄ and related species: linking transport, surface
836 flux and chemical loss with CH₄ variability in the troposphere and lower
837 stratosphere. *Atmospheric Chemistry and Physics* 11, 12813-12837.

838 Pickers, P.A., Manning, A.C., 2015. Investigating bias in the application of curve fitting
839 programs to atmospheric time series. *Atmospheric Measurement Techniques* 8,
840 1469-1489.

841 Rafter, T.A., 1955. ¹⁴C variations in nature and the effect on radiocarbon dating. *New*
842 *Zealand Journal of Science and Technology* B37.

843 Rafter, T.A., Fergusson, G., 1959. Atmospheric radiocarbon as a tracer in geophysical
844 circulation problems, United Nations Peaceful Uses of Atomic Energy. Pergamon
845 Press, London.

846 Randerson, J.T., Enting, I.G., Schuur, E.A.G., Caldeira, K., Fung, I.Y., 2002. Seasonal
847 and latitudinal variability of troposphere Δ¹⁴CO₂: Post bomb contributions from
848 fossil fuels, oceans, the stratosphere, and the terrestrial biosphere. *Global*
849 *Biogeochemical Cycles* 16, 1112.

850 Reimer, P.J., Brown, T.A., Reimer, R.W., 2004. Discussion: Reporting and calibration of
851 post-bomb ¹⁴C data. *Radiocarbon* 46, 1299-1304.

852 Rodgers, K.B., Mikaloff-Fletcher, S.E., Bianchi, D., Beaulieu, C., Galbraith, E.D.,
853 Gnanadesikan, A., Hogg, A.G., Iudicone, D., Lintner, B.R., Naegler, T., Reimer,
854 P.J., Sarmiento, J.L., Slater, R.D., 2011. Interhemispheric gradient of atmospheric
855 radiocarbon reveals natural variability of Southern Ocean winds. *Climate of the*
856 *Past* 7, 1123-1138.

857 Sitch, S., Friedlingstein, P., Gruber, N., Jones, S.D., Murray-Tortarolo, G., Ahlström, A.,
858 Doney, S.C., Graven, H., Heinze, C., Huntingford, C., Levis, S., Levy, P.E., Lomas,
859 M., Poulter, B., Viovy, N., Zaehle, S., Zeng, N., Arneeth, A., Bonan, G., Bopp, L.,
860 Canadell, J.G., Chevallier, F., Ciais, P., Ellis, R., Gloor, M., Peylin, P., Piao, S.L.,
861 Le Quéré, C., Smith, B., Zhu, Z., Myneni, R., 2015. Recent trends and drivers of
862 regional sources and sinks of carbon dioxide. *Biogeosciences* 12, 653-679.

863 Steinkamp, K., Mikaloff Fletcher, S.E., Brailsford, G., Smale, D., Moore, S., Keller,
864 E.D., Baisden, W.T., Mukai, H., Stephens, B.B., 2017. Atmospheric CO₂
865 observations and models suggest strong carbon uptake by forests in New Zealand.
866 *Atmospheric Chemistry and Physics* 17, 47-76.

867 Stephens, B.B., Brailsford, G.W., Gomez, A.J., Riedel, K., Mikaloff Fletcher, S.E.,
868 Nichol, S., Manning, M., 2013. Analysis of a 39-year continuous atmospheric CO₂
869 record from Baring Head, New Zealand. *Biogeosciences* 10, 2683-2697.

870 Stuiver, M., Polach, H.A., 1977. Discussion: Reporting of ¹⁴C data. *Radiocarbon* 19, 355-
871 363.

872 Stuiver, M., Quay, P.D., 1981. Atmospheric 14C changes resulting from fossil fuel CO₂
873 release and cosmic ray flux variability. *Earth and Planetary Science Letters*, 53,
874 349-362.

875 Suess, H.E., 1955. Radiocarbon concentration in modern wood. *Science* 122, 414-417.

876 Sweeney, C., Gloor, E., Jacobson, A.R., Key, R.M., McKinley, G., Sarmiento, J.L.,
877 Wanninkhof, R., 2007. Constraining global air-sea gas exchange for CO₂ with
878 recent bomb ¹⁴C measurements. *Global Biogeochemical Cycles* 21.

879 Tans, P.P., De Jong, A.F., Mook, W.G., 1979. Natural atmospheric ¹⁴C variation and the
880 Suess effect. *Nature* 280, 826-828.

881 Thoning, K.W., Tans, P.P., Komhyr, W.D., 1989. Atmospheric carbon dioxide at Mauna
882 Loa Observatory 2. Analysis of the NOAA GMCC data, 1974-1985. *Journal of*
883 *Geophysical Research* 94, 8549-8563.

884 Trumbore, S.E., 2000. Age of soil organic matter and soil respiration: Radiocarbon
885 constraints on belowground C dynamics. *Ecological Applications* 10, 399-411.

886 Turnbull, J.C., 2006. Development of a high precision ¹⁴CO₂ measurement capability and
887 application to carbon cycle studies, Geological Sciences. University of Colorado,
888 Boulder, p. 132.

889 Turnbull, J.C., Miller, J.B., Lehman, S.J., Hurst, D.F., Peters, W., Tans, P.P., Southon,
890 J.R., Montzka, S.A., Elkins, J.W., Mondeel, D.J., Romashkin, P.A., Elansky, N.F.,
891 Shkorokhod, A., 2009. Spatial distribution of Δ¹⁴CO₂ across Eurasia:
892 Measurements from the TROICA-8 expedition. *Atmospheric Chemistry and*
893 *Physics* 9, 175-187.

894 Turnbull, J.C., Rayner, P.J., Miller, J.B., Naegler, T., Ciais, P., Cozic, A., 2009. On the
895 use of ¹⁴CO₂ as a tracer for fossil fuel CO₂: quantifying uncertainties using an
896 atmospheric transport model. *Journal of Geophysical Research* 114, D22302.

897 Turnbull, J.C., Sweeney, C., Karion, A., Newberger, T., Lehman, S.J., Tans, P.P., Davis,
898 K.J., Lauvaux, T., Miles, N.L., Richardson, S.J., Cambaliza, M.O., Shepson, P.B.,
899 Gurney, K., Patarasuk, R., Razlivanov, I., 2015. Toward quantification and source
900 sector identification of fossil fuel CO₂ emissions from an urban area: Results from
901 the INFLUX experiment. *Journal of Geophysical Research: Atmospheres*.

902 Turnbull, J.C., Zondervan, A., Kaiser, J., Norris, M., Dahl, J., Baisden, W.T., Lehman,
903 S.J., 2015. High-precision atmospheric ¹⁴CO₂ measurement at the Rafter
904 Radiocarbon Laboratory. *Radiocarbon* 57, 377-388.

905 Wang, Y., Li, M., Shen, L., 2013. Accelerating carbon uptake in the Northern
906 Hemisphere: evidence from the interhemispheric difference of atmospheric CO₂
907 concentrations. *Tellus B* 65.

908 Ziehn, T., 2014. Greenhouse gas network design using backward Lagrangian particle
909 dispersion modelling – Part 1: Methodology and Australian test case. *Atmospheric*
910 *Chemistry and Physics* 14.

911 Zondervan, A., Hauser, T., Kaiser, J., Kitchen, R., Turnbull, J.C., West, J.G., 2015.
912 XCAMS: The compact ¹⁴C accelerator mass spectrometer extended for 10Be and

913 ²⁶Al at GNS Science, New Zealand. Nuclear Instruments and Methods B361, 25-
914 33.
915 Zondervan, A., Sparks, R.J., 1996. Development plans for the AMS facility at the
916 Institute of Geological and Nuclear Sciences, New Zealand. Radiocarbon 38, 133-
917 134.
918

919 **10. Tables**

920
921
922

Sampling Date Range	Sample ID NZ/NZA	Site	collection method	Measurement method
1954-1986	0-7500	MAK	tray	Gas counting
1987-1994	7500-8400	BHD	tray	Gas counting
1995-2004	8400-30000	BHD	bottle	AMS ENTandem ¹³ C ¹⁴ C
2005-2009	30000-34000	BHD	bottle	AMS ENTandem ¹² C ¹³ C ¹⁴ C
2010-2011	34000-50000	BHD	bottle	AMS XCAMS
2012-present	50000-	BHD	bottle	AMS XCAMS/RG20

923 **Table 1.** Wellington ¹⁴CO₂ measurement methods through time. Gas counting samples
924 are identified by NZ numbers, AMS samples by NZA numbers. NZ and NZA numbers
925 do not overlap. Sites are Makara (MAK) and Baring Head (BHD). Collection and
926 measurement methods are described in detail in the text.

927
928
929

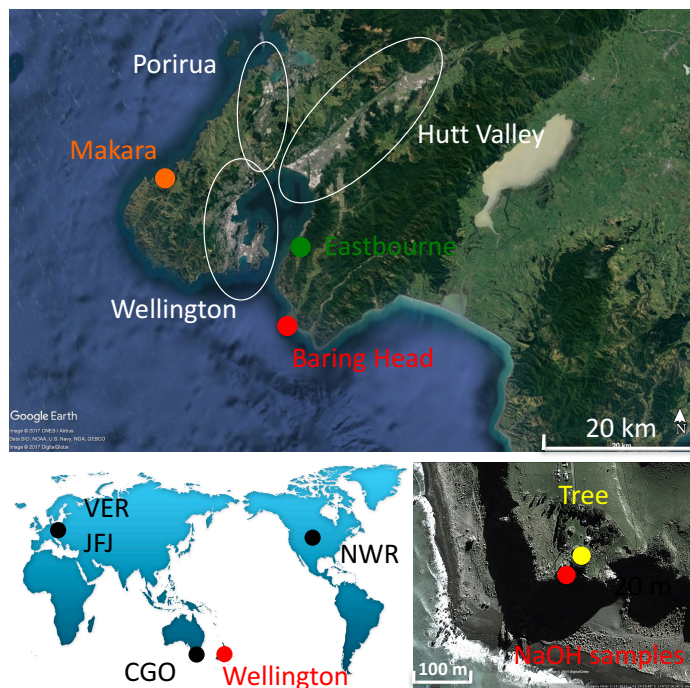
Site difference	Time period	$\Delta^{14}\text{CO}_2$ difference (‰)
BHD-CGO	1986-1990	1.8 ± 2.5
BHD-CGO	2005-2013	1.3 ± 3.4
BHD-JFJ	1986-1990	0.8 ± 3.9
BHD-JFJ	2005-2013	4.8 ± 2.7
BHD-NWR	2005-2013	6.9 ± 2.5

930 **Table 2.** $\Delta^{14}\text{CO}_2$ gradients between sites, determined as the mean of the monthly
931 differences for each time period. Errors are the standard deviation of the monthly
932 differences.
933

934 11. Figures

935

936



937

938 **Figure 1.** Sampling locations. Top: Makara (1954-1986) and Baring Head (1987 –

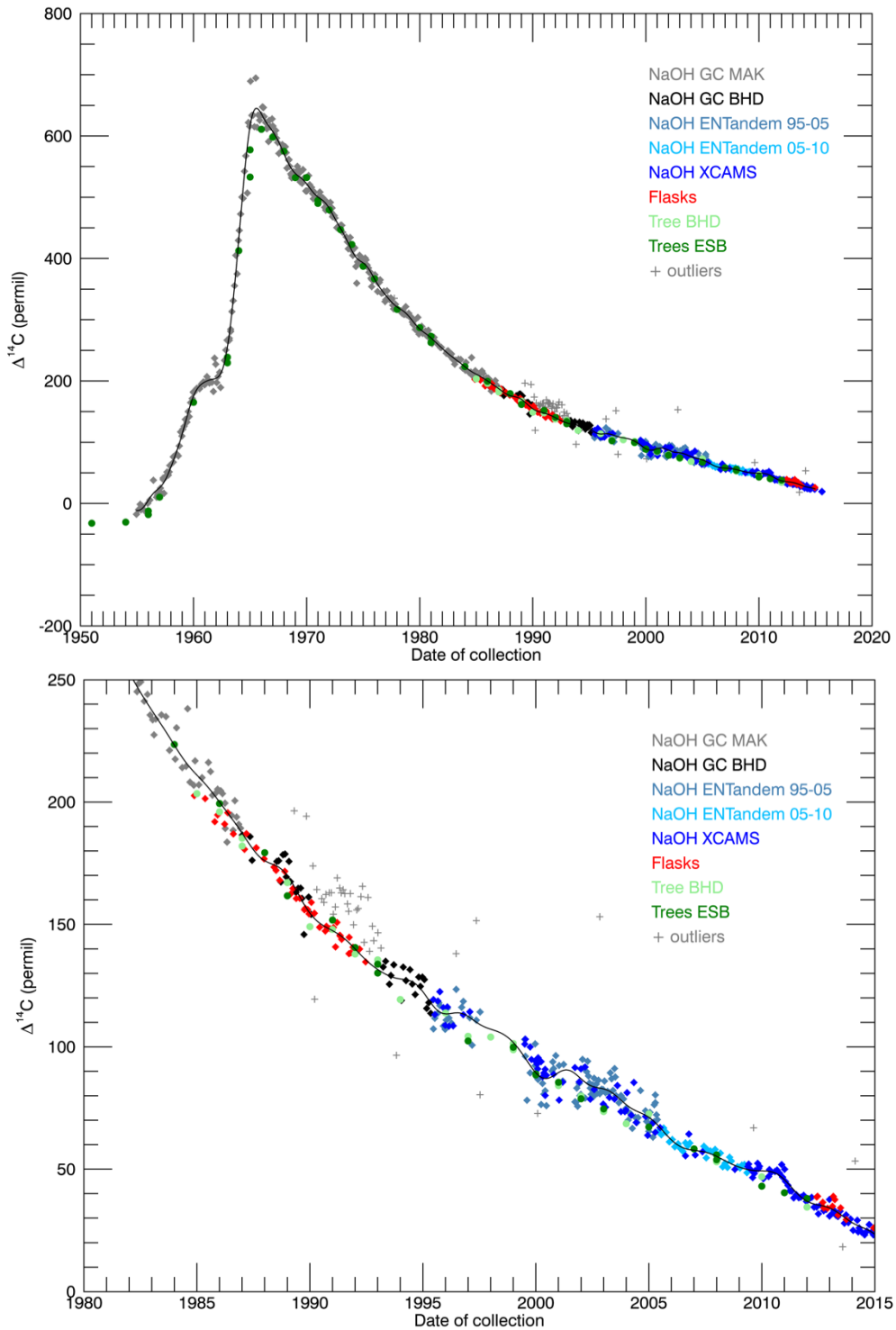
939 present) air sampling sites, the location of the Eastbourne tree samples, and the urbanized

940 areas of Wellington, Porirua and the Hutt Valley. Bottom left: world location showing

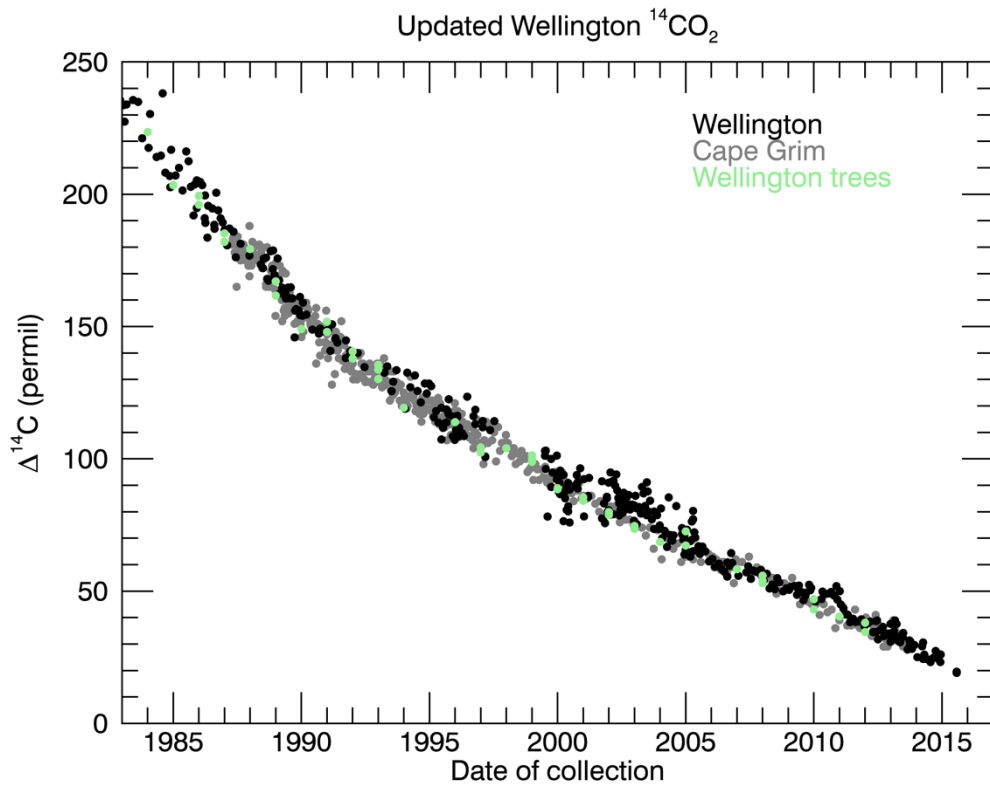
941 Wellington and other sampling sites discussed in the text. Bottom right: close up of the

942 Baring Head site showing the relative positions of the air (NaOH) and tree sampling

943 locations.



944
 945 **Figure 2.** Wellington $^{14}\text{CO}_2$ record showing all collection and measurement methods for
 946 the full record (top) and zoomed in for the period since 1980 (bottom). Tree rings (green)
 947 and outliers (grey pluses) are excluded from the reported final dataset. Black line is the
 948 smooth curve fit to the final dataset.
 949

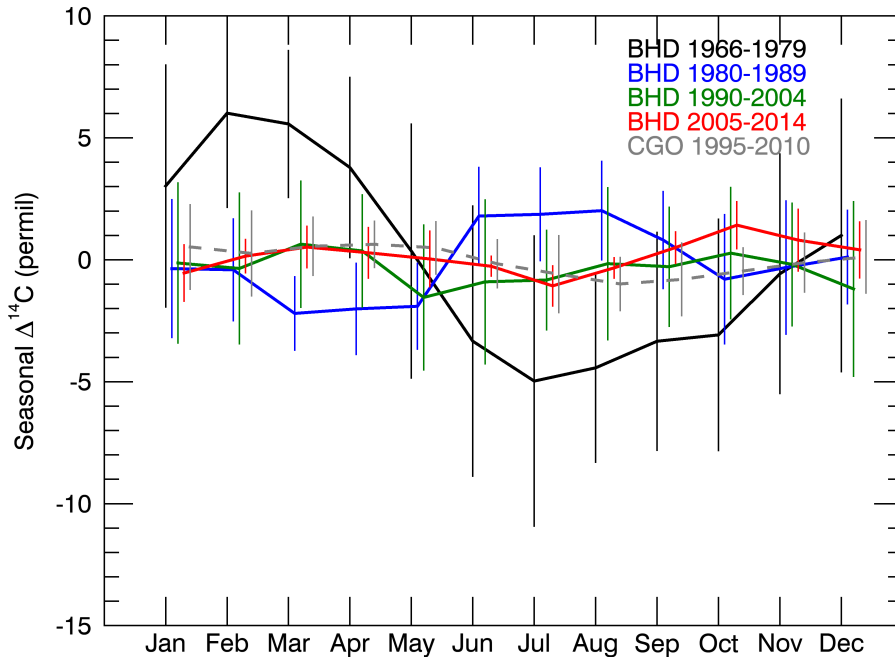


950

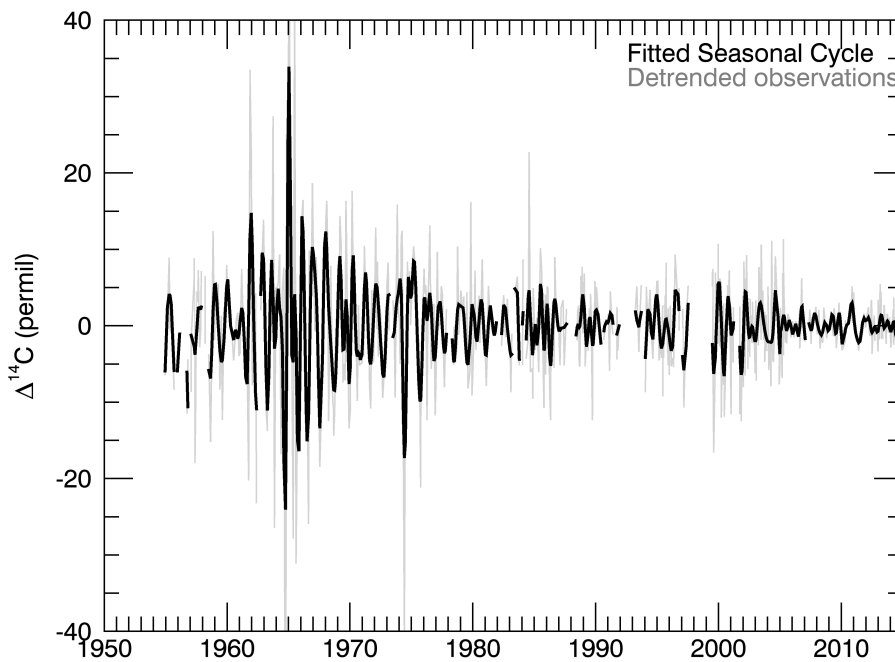
951

952 Figure 3. Comparison of the final Wellington and Cape Grim (Levin et al., 2010) Δ¹⁴CO₂

953 records. Wellington tree ring measurements are also shown.

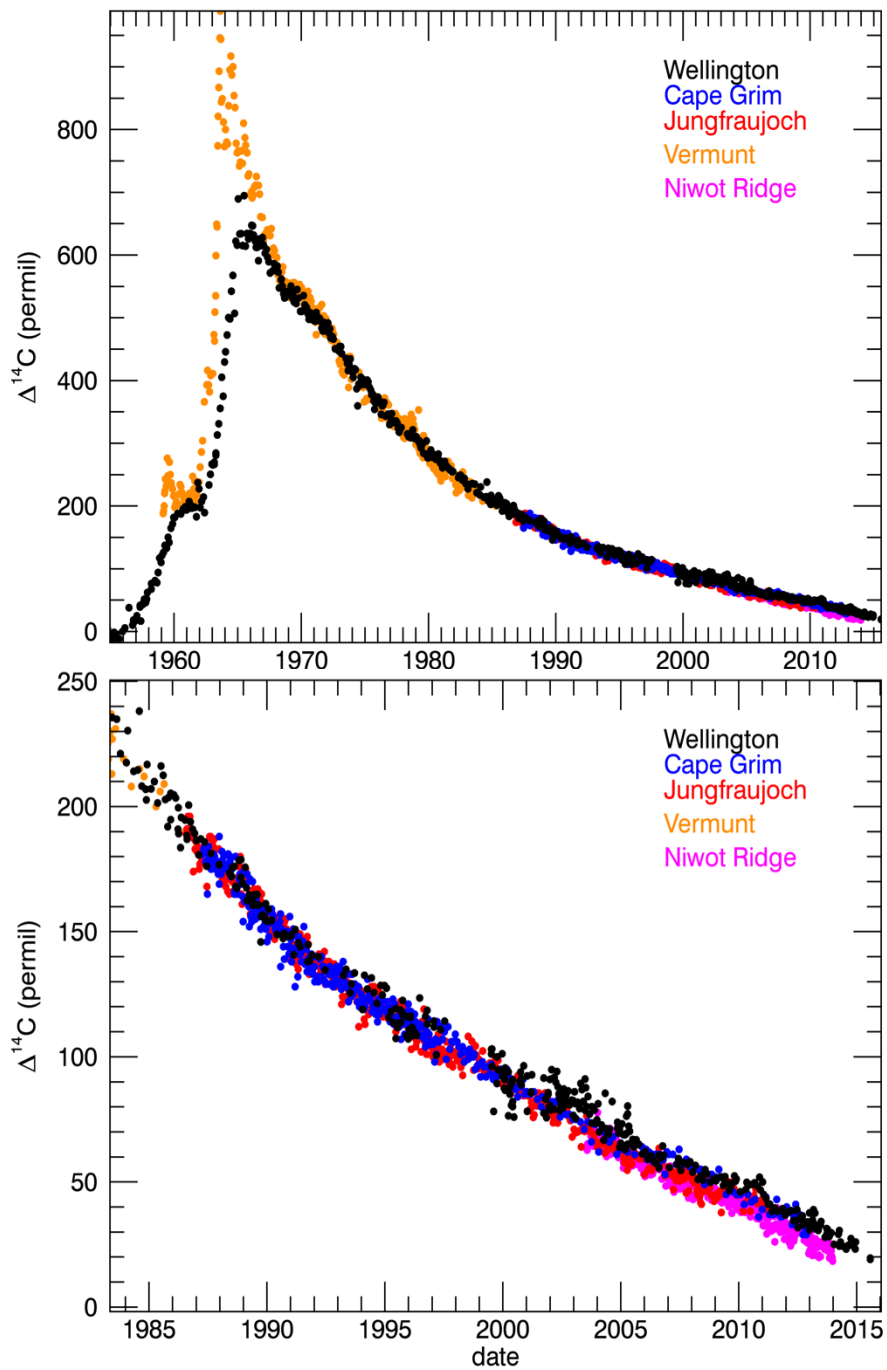


954



955

956 Figure 4. Detrended seasonal cycle in the Wellington $\Delta^{14}\text{CO}_2$ record. Top: BHD
 957 monthly detrended seasonal cycle averaged over four time periods as described in the text
 958 and the CGO (Levin et al., 2010) detrended seasonal cycle. Error bars are the standard
 959 deviation of all years averaged. Points for each time period are slightly offset for clarity.
 960 Bottom: full seasonal cycle record determined separately for each time period shown in
 961 the top panel plus 1954-1965 (black) and detrended observations without any smoothing
 962 (grey).



964
965
966
967
968

Figure 5. Comparison of Wellington and other atmospheric $\Delta^{14}\text{CO}_2$ records (Levin et al., 2010; Turnbull et al., 2007; Lehman et al., 2013).